Hydrogen production by hydrothermal oxidation of FeO under acidic conditions

Camille Crouzet, Fabrice Brunet, Nadir Recham, N. Findling, M Lanson, François F Guyot, Jean-Henry Ferrasse, Bruno Goffé

Hydrogen production by hydrothermal oxidation of FeO under acidic conditions

C. Crouzet [a,b,d,*], F. Brunet [a], N. Recham [b], N. Findling [a], M. Lanson [a], F. Guyot [c], J.-H. Ferrasse [d], B. Goffe [e]

[a] Universite Grenoble Alpes, CNRS, ISTerre, Maison des Geosciences, F-38000 Grenoble, France
[b] Laboratoire de Reactivite et Chimie des Solides (LRCS), Universite de Picardie Jules Verne, CNRS UMR 7314, 80039 Amiens Cedex, France
[c] Institut de mineralogie, de physique des materiaux et de cosmochimie, Sorbonne Universite, Museum National d'Histoire Naturelle, UMR 7590, CNRS, UPMC, MNHN, IRD, F-75005 Paris, France
[d] Mecanique, Modelisation & Procedes Propres (M2P2), Aix-Marseille Universite, Centrale Marseille, CNRS, M2P2 UMR 7340, Europôle de l'Arbois, 13545 Aix-en-Provence Cedex 4, France
[e] CEREGE, Aix-Marseille Universite, CNRS UMR 7330, Europôle de l'Arbois, 13545 Aix-en-Provence, France

Keywords:
Hydrogen production
FeO oxidation
Steel slags
Hydrothermal conditions
Acetic acid

The production of H_2 by oxidation of FeO, taken here as model compound for steel slags, has been investigated both in pure water and under acidic aqueous conditions in the 373 e573 K temperature range. Whereas after 65 h, H_2 yield was negligible in pure water at 423 K, the reaction $3\,FeO_{(s)} + H_2O_{(l)} = Fe_3O_{4(s)} + H_{2(aq)}$ reached near completion at the same temperature within 10 h in a solution containing 0.05 mol/l acetic acid. Increasing acetic acid concentration by one order of magnitude did not yield significantly more H_2. At identical initial pH, acetic acid was found to be more efficient than oxalic acid and hydrochloric acid at enhancing H_2 production. Acidic conditions increased FeO dissolution kinetics and, consequently, improved H_2 yield. The specific efficiency of acetic acid resides in its thermal stability as well as in the potential of ligand-promoted Fe(II) dissolution. We show that the positive kinetics effect of mild acetic acid solutions over H_2 yield evidenced on FeO does not apply directly to steel slags which buffer the pH to high values due to the presence of large amounts of CaO.

Introduction

Among alternative energy sources, dihydrogen (H_2) has an important role to play, especially with the development of fuel cell technologies. Nowadays, two main processes are used to produce H_2 with the required purity, steam methane reforming with an additional purification step and water electrolysis. However, with the aim of developing new sustainable hydrogen production methods, alternative ways are also being investigated. For example, extensive research is being carried out on hydrogen production from biomass and processes based on the use of renewable energy sources for electrolysis or thermochemical cycle paths [1e3]. The H_2 production method presented here is inspired from an

* Corresponding author. Present address: ISTerre, Maison des Geosciences, BP 35, F-38041 Grenoble Cedex 9, France.
E-mail address: camille.crouzet@univ-grenoble-alpes.fr (C. Crouzet).

abiogenic geochemical process which corresponds to the formation of native dihydrogen by interaction between rock and hot seawater at mid-oceanic ridges. Under these natural hydrothermal conditions, H_2 is a by-product of the hydration of olivine $(Mg, Fe)_2SiO_4$, the main mineral constituent of the Earth's upper-mantle. Ferrous iron contained in olivine is partly incorporated as Fe^{3+} in magnetite in the course of these hydration reactions (serpentinization) which take place in the oceanic crust [4e6]. Malvoisin et al. (2013, [7]) showed that high-purity hydrogen can be produced from steel slag, a massive steel industry by-product, under the pressure and temperature conditions of serpentinization, i.e., 350 C and 50 MPa, by oxidation of the iron (II) contained by wüstite (Fe, Mg)O, in steel slags and by the subsequent reduction of water [7]. This method of geo-inspired H_2 production from steel slags, is also reminiscent of the H_2 production method used at the beginning of the 20th century. Hydrogen was produced from 823 to 1173 K according to the so-called steam-iron process based on the same iron-oxidation principle, through cycles of iron metal oxidation in the presence of steam and iron oxide reduction by gasified coal [8e11]. More recently, several studies have focused on chemical looping combustion (CLC). CLC is a cyclic route where metal oxide particles, such as iron oxides, are reduced during the combustion in a fuel reactor and then re-oxidized in a second air reactor. If this method was first developed to capture the CO_2 produced by the fuel combustion, this process can also be used to produce H_2 by performing the oxidation step in the presence of steam [12e15].

Following the work by Malvoisin et al. (2013, [7]) on steel slags, we investigated here the role of acidic conditions on hydrogen yield and production kinetics from pure FeO oxidation. Due to the complex chemistry of slags, we focused here on the behavior of pure FeO in order to unravel the chemical processes which lead to H_2 production. A few additional experiments were however performed by adding CaO, the main constituent of steel slags, in order to approach FeO behavior in steel-slag-like compositions. Initially present in the form of lime in fresh slags, CaO transforms into Ca-hydroxide and carbonate by aging in air. Therefore, the CaO component was introduced either in the form of $Ca(OH)_2$ or $CaCO_3$ in these additional experiments.

The role of pH on H_2 production kinetics is somehow difficult to predict. H_2 production from FeO interaction with water is the result of at least two steps, wüstite dissolution and magnetite precipitation. Between these two steps, ferrous iron must be partly oxidized into ferric iron. Potentially, each of these three steps (FeO dissolution, Fe^{2+} oxidation and Fe_3O_4 precipitation) can be rate limiting. Indeed, low pH has been shown to favor Fe solubilization [16] which may have a positive effect on H_2 yield. Precipitation of iron oxides (and hydroxides) by oxidation of aqueous ferrous salts has been extensively studied [17]. Properties of the solvent (ionic strength) and the nature of the ion pair have a clear influence on the kinetics of aqueous Fe(II) oxidation. It has also been shown that Fe(II) aqueous oxidation kinetics by O_2 is positively correlated to pH for $4 < pH < 8$ [18]. Furthermore, surface of hydrous oxides can catalyze the redox process (auto-oxidation process, [19,20]). All these studies, however, were performed at ambient conditions, and little is known about Fe(II) aqueous oxidation at higher temperature and pressure.

Materials and methods

Starting materials

Reagent grade wüstite, FeO (99.9%, ALDRICH®), was crushed and sieved to a particle size of 50e100 mm with a specific surface area of 0.70 m^2/g as measured by N_2-BET. The oxidation state of iron in the starting material was quantified by Mössbauer spectroscopy to be 91.6% Fe^{2+}, 5.6% Fe^{3+} and 2.8% Fe^0. Average iron oxidation state corresponds to pure Fe(II), consistent with the FeO reagent grade. Both ferric iron and metal iron are residues of industrial FeO synthesis which consists in a high temperature reaction between iron metal and hematite (Fe_2O_3).

Sealed gold capsules

A set of experiments was performed in cold-seal vessels. The starting material (80 mg) was loaded in a gold tube (4.0 mm outer diameter and 3.6 mm inner diameter) with de-ionized water in a constant mass ratio of 1:1. The two ends of the tube were welded shut to form a capsule which was placed in the pressure vessel, itself introduced in a horizontal furnace. Temperatures in the 373e473 K range were investigated at 30 MPa argon pressure. Since gold is ductile, the water pressure in both the autoclave and the inner capsule pressure are the same (see Brunet and Chopin (1996, [21]) for experimental details); this pressure is kept constant all along the experiments. At the end of experiment, the pressure vessel was quenched under a compressed air stream. This type of experiment is easy to set-up and several samples can be run in a raw. It is therefore convenient to investigate the effect of temperature or acid concentration on H_2 yield in a minimum amount of time. On the other hand, compared to the sampling autoclave, (1) only large starting material: water ratio can be investigated (typically 1:1), (2) fluids cannot be sampled in-situ and can only be analyzed at the end of the run. The gas produced by the sample and enclosed in the gold capsule is

recovered following the method described in Malvoisin (2013, [7]) and injected with a syringe through the septum of a gas chromatograph for analysis.

Sampling autoclave

Another set of experiments was carried out with a sampling autoclave in order to allow time-resolved monitoring of the H_2 production. A 500 mL autoclave made of hastelloy™ (nickel based alloy) is equipped with a set of high-pressure connec-tions for gas and solution sampling (Fig. 1). The autoclave is heated by two tight resistive collars (upper and lower). Both gas and aqueous solutions are stirred at a speed of 800 rpm. The experiments were carried out with a solid: solution mass ratio of 1:200.

HP-HT gas is sampled in a water-cooled condenser prior to its injection in the gas chromatograph (GC) for analysis. The
aqueous solution is sampled through a plunging capillary and

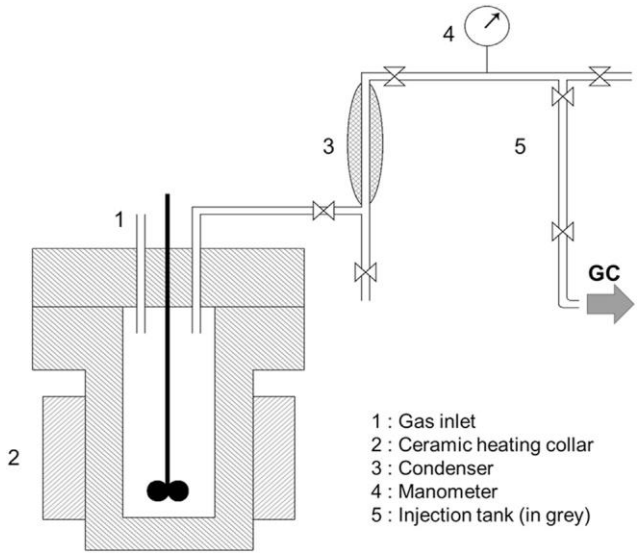

Fig. 1 e 500 mL stirred autoclave with aqueous and gas sampling directly plugged to the gas chromatograph (GC).

filtered at high pressure and high temperature by a titanium frit with 0.2 mm pores. Sampled solutions were stored in a fridge until they were analyzed using ICP.

Analysis of the fluids

Gas components (H_2, CO_2, N_2, O_2, CO, CH_4) were analyzed with a Clarus 500 gas chromatograph (Perkin Elmer®) equipped with a polymer filled column (Restek ShinCarbon®) and a thermal conductivity detector (TCD). The temperature of the detector, the injection system and the oven were respectively set to 523, 373 and 353 K. Argon was used as gas carrier. Each gas sample was analyzed at least three times consecutively.

Iron content in the solution was determined right after sampling, on 2 mL aliquots, by UV-spectroscopy after complexation by orthophenantroline. This method allowed a fast quantification, compatible with the sampling frequency, with a detection limit of 0.1 ppm. Kept in the fridge, all solutions were measured at another time for total iron content by ICP-OES.

Solid characterization

The recovered solid products were first washed through repeated water rinsing and then crushed for X-ray powder diffraction (XRPD). XRPD patterns were collected with a D8 diffractometer (Bruker, CuKa radiation) operated with a 2q step size of 0.026 and a counting time of 8 s.

Part of the recovered solid sample was kept unground for further electron microscopy characterization, Field Emission Scanning Electron Microscopy (FE-SEM) and Transmission Electronic Microscopy (TEM). FE-SEM characterization was performed with a ZEISS Ultra 55 using both secondary and back-scattered electrons. TEM was performed on a Jeol FEG 2100F operated at 200 kV. Both FE-SEM and TEM were equipped with an Energy-Dispersive X-ray spectroscopy (EDS) detector for chemical analysis. For FE-SEM characterization, prior to carbon coating, the sample was either mounted on a double-sided carbon tape or embedded in epoxy and polished. For TEM, a drop of the powder sample dispersed in ethanol was deposited on a Lacey carbon-coated grid.

Derivation of total H_2 production from the experimental data

In the case of the experiments performed in sealed gold capsules, the sample is quenched before the capsule is pierced and the gas is sampled and analyzed. Owing to the limited solubility of H_2 in water at ambient conditions, it can be considered that all the H_2 produced in the experiments is concentrated, at ambient conditions, in the gas phase. The situation is totally different in the case of sampling autoclave experiments where the gas phase is sampled at high T and P. A significant amount of H_2 may be concentrated in the solution. The H_2 distribution between gas and solution can be estimated by using the Henry's law constant and its temperature dependency as calculated using the SUPCRT92 database [22]. Furthermore, multiple sampling of the gas phase leads to a progressive extraction of H_2 from the system, which must also be taken into account.

Finally, it is convenient to express the total H_2 production as H_2 produced per kg of initial FeO according to reaction:

$$3FeO_{(s)} + H_2O_{(l)} = Fe_3O_{4(s)} + H_{2(aq)} \quad (1)$$

Reaction progresses are therefore calculated as the amount of H_2 produced per kg of FeO in the starting material divided by 9.28 g of H_2 per kg of FeO. However, in the case of experiments performed at low pH, part of the iron introduced in the system is sequestered as aqueous Fe^{2+} due to the reaction:

$$FeO_{(s)} + 2H^+_{(aq)} = Fe^{2+}_{(aq)} + H_2O_{(l)} \quad (2)$$

and will not be available for H_2 production or magnetite. Consequently, in order to compare at various pH values the extent of Reaction (1) derived from H_2 content in the gas phase, a correction for Fe^{2+} has been applied.

Thermodynamic background

Stability of iron oxides in water has been calculated at 423 K and 20 MPa, in the absence of a gas phase; using the SUPCRT92 thermodynamic database. Two types of reactions have been considered, redox reactions among iron oxides, e.g., Reaction (1) and oxide e water equilibria, e.g., Reaction (2). Aqueous Fe^{3+} was neglected since it is far less abundant than Fe^{2+}. Consequently, oxide e water equilibria involving iron oxides containing ferric iron are also redox reactions, e.g.,

$Fe_3O_{4ðsÞ}$ þ $H_{2ðaqÞ}$ þ $6H^{þ}_{ðaqÞ}$%$3Fe^{2þ}_{ðaqÞ}$ þ $4H_2O_{ðlÞ}$: The system is defined by three activity variables, $a_{Hþ}$, $a_{H_{2;aq}}$ and $a_{Fe^{2þ}}$. All equilibria can be plotted in a $\log a_{Fe2þ}=a_{Hþ}^{2}$ $\log a_{H_{2aq}}$ diagram (Fig. 2). In this diagram, the $H_{2(aq)}$ % $H_{2(g)}$ equilibrium boundary falls in a range of $H_{2\ (aq)}$ activity where Fe_3O_4 is stable meaning that the triple point $FeO_{(s)}eFe_3O_{4(s)}eFe^{2þ}_{(aq)}$ will never be reached when reacting FeO with water (see so-
lution reaction path, Fig. 2). In other words, at constant

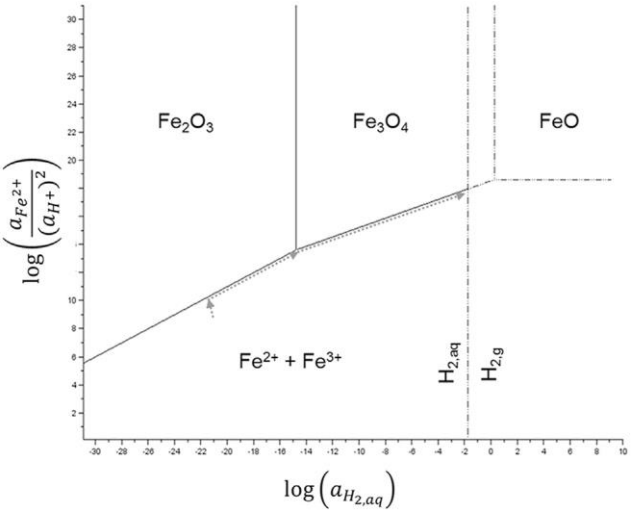

Fig. 2 e Stability diagram of iron oxides in water as a function of the activity of dissolved Fe^{2+} activity divided by squared H^+ activity and the activity of dissolved H_2. The dotted line corresponds to the solution reaction path followed by an "oxidized" solution to which FeO is added as calculated with PHREEQC [32]. Hematite (Fe_2O_3) saturation will first be reached. Then, assuming that hematite nucleation and growth kinetics are not limiting, FeO dissolution will be accompanied by Fe_2O_3 precipitation and H_2 production. The solution will get enriched in $H_{2(aq)}$ and will evolve on the Fe_2O_3 saturation line up to the triple point, Fe_2O_3 e Fe_3O_4 e aqueous species. At this point, hematite should be totally converted into magnetite before FeO dissolution allows the solution to get further enriched in $H_{2(aq)}$. Magnetite and $H_{2,aq}$ are produced until $H_{2(g)}$ saturation is achieved. At H_2 saturation, further Fe_3O_4 formation is accompanied by $H_{2(g)}$ production. If P and T are kept constant then $a_{H_{2;aq}}$ in the aqueous solution is fixed. Note that the triple point FeOeFe_3O_4-aqueous species is never reached, meaning that FeO saturation will not be achieved.

pressure and temperature, FeO will never be stable with water and should therefore react until disappearance.

Results

Sealed gold capsules

Acetic, oxalic and hydrochloric acid solutions were prepared at concentrations of 0.05, 0.001 and 0.001 mol/L respectively, corresponding to a starting pH of 3. These solutions were sealed together with unsieved FeO powder from the same starting material in gold capsules and reacted for 10 days at 423 K and 30 MPa. After quenching, the capsule containing acetic acid was significantly more inflated than the others. The amount of H_2 recovered from acetic acid experiments was about 10 times higher than in experiments with hydrochloric and oxalic acids (Fig. 3).

Three experiments were prepared with the same protocol but with acetic acid concentrations of 0.005, 0.05 and 0.5 mol

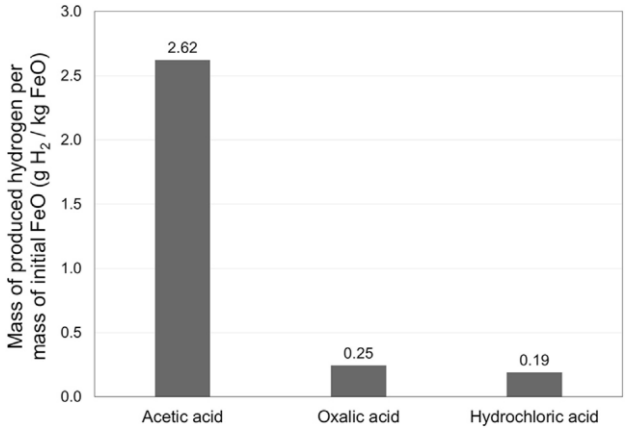

Fig. 3 e Comparison of hydrogen production between three different acids after 11 days of reaction (423 K e 30 MPa).

per liter corresponding to starting pH of 3.5, 3.0, 2.5, respectively. After three days at 423 Ke30 MPa, only 0.074 g H_2/kg FeO was produced for the 0.005 mol/L experiment whereas 2.58 and 1.91 g H_2/kg FeO were recovered for initial acetic acid concentrations of 0.05 and 0.5 mol/L, respectively, i.e., about 25% of reaction. For these two experiments, the final pH values are calculated to be 5.0, 4.7 and 4.5, respectively.

Three run temperatures were tested at 30 MPa, 373, 423 and 473 K with capsules containing FeO and acetic acid at a concentration of 0.05 mol/L and for run durations from 3 to 172 h (Table 1, Fig. 4). After 72 h, the amount of H_2 produced at 373, 423 and 473 K resulted, respectively, in 0.058, 2.58 and 5.34 g H_2/kg FeO (Table 1). Data could not be successfully fitted to a first-order kinetic model, a square root function yielded better fits (Fig. 4) which allowed to derive an activation energy of 27 kJ/mol.

Sampling autoclave: effect of pH

Two experiments were conducted by introducing FeO in distilled water at 423 and 573 K in the sampling autoclave. Hydrogen was produced at both temperatures following two different kinetic models. At 423 K, after a first period of hydrogen production in the first 10 h up to a value of 0.14 g H_2/kg FeO, H_2 production ceased (Fig. 5). Magnetite grains were identified through XRPD. At 573 K, corrected H_2 production increased during the first 24 h and slowed down progressively to reach 1.28 g H_2/kg FeO after 144 h. Maximum H_2 production is equivalent to 23% of the reaction progress. H_2 production at 573 K has been fitted to a pseudo first-order kinetics (Fig. 5). In both experiments, iron (II) concentration was too low to be detected by UV-spectrophotometry. Calculations using PHREEQC predicted a concentration of around 10^{-7} mol per liter at 573 K, i.e., far below the detection limit of UV-spectrophotometry.

FeO dissolution in aqueous solution containing 0.05 mol/L acetic acid was monitored in a sampling autoclave by analyzing aqueous Fe^{2+} and H_2 in the gas phase. FeO dissolution occurred according to a two-step process (Fig. 6a). Fast dissolution was encountered during the first 10 h until a maximum [Fe^{2+}] concentration of about 0.02 mol/L was reached. At this stage, more than 10%$_w$ of the initial sample had dissolved. Within the next following 10 h [Fe^{2+}] decreased to reach a plateau at 0.01 mol/L. It

Table 1 – Experimental conditions, H_2 yield (GC) and presence of iron oxides (besides FeO and Fe_3O_4) as detected by XRPD.

Sample name	Method	Solution	Concentration (mol/L)	Temperature (K)	Pressure (MPa)	End time (hours)	Starting solution pH[a]	Normalized hydrogen production at theend of experiment[b] (g H_2/kg FeO – g/kg)	Goethite (G) or Lepidocrocite (L) FeO(OH) presence[c]
CT-H2-Ac[d]	Capsule	Acetic acid	0.05	423	30	240	3	2.62 (28%)	–
CT-H2-Ox[d]	Capsule	Oxalic acid	0.001	423	30	240	3	0.24 (3%)	–
CT-H2-HCl[d]	Capsule	HCl	0.001	423	30	240	3	0.20 (2%)	–
CAc-H2_01	Capsule	Acetic acid	0.005	423	30	72	3.5	0.074 (1%)	–
CAc-H2_02	Capsule	Acetic acid	0.05	423	30	72	3	2.58 (28%)	–
CAc-H2_03	Capsule	Acetic acid	0.5	423	30	72	2.5	1.91 (21%)	G
CAc-H2_04	Capsule	Acetic acid	0.05	373	30	72	3	0.058 (<1%)	G
CAc-H2_05	Capsule	Acetic acid	0.05	473	30	72	3	5.34 (58%)	L
CAc-H2_06	Capsule	Acetic acid	0.05	423	30	24	3	1.34 (14%)	G þ L
CAc-H2_07	Capsule	Acetic acid	0.05	423	30	3	3	0.068 (<1%)	G
CAc-H2_08	Capsule	Acetic acid	0.05	423	30	168	3	4.08 (44%)	–
CAc-H2_10	Capsule	Acetic acid	0.05	423	30	72	3	2.46 (27%)	–
CAc-H2_12	Capsule	Acetic acid	0.05	423	30	8	3	0.30 (3%)	G
CAc-H2_13	Capsule	Acetic acid	0.05	373	30	172	3	0.23 (2%)	G
CAc-H2_14	Capsule	Acetic acid	0.05	473	30	24	3	3.74 (40%)	L
CAc-H2_15	Capsule	Acetic acid	0.05	473	30	3	3	2.86 (31%)	–
CAc-H2_16	Capsule	Acetic acid	0.05	473	30	48	3	3.26 (35%)	–
CHCl-H2_11	Capsule	HCl	0.001	423	30	72	3	0.084 (<1%)	–
CHCl-H2_17	Capsule	HCl	0.001	473	30	72	3	0.19 (2%)	–
CAc-$Ca(OH)_2$	Capsule	Acetic acid þ $Ca(OH)_2$*	0.05	423	30	72	3	0.0005 (<1%)	–
CAc-$CaCO_3$	Capsule	Acetic acid þ $CaCO_3$*	0.05	423	30	72	3	0.05 (<1%)	–
APAc-H2-150	Sampling autoclave	Acetic acid	0.05	423	16	48	3	8.06[e] (87%)	–
APW-H2-150	Sampling autoclave	Water	–	423	15	64.5	6	0.26[e] (3%)	–
APW-H2-300	Sampling autoclave	Water	–	573	18	144	6	2.18[e] (23%)	–

*Additional solid unused for starting pH calculations.

[a] Starting pH calculated from acidic solution initial concentration.

[b] Mass of H_2 produced deduced by gas chromatography divided by initial mass of solid reagent, calculated reaction progresses are presented in brackets.

[c] Observation or not of goethite and/or lepidocrocite by XRPD on retrieved solid samples.

[d] Experiments conducted on unsieved starting materials.

[e] Corrected hydrogen production.

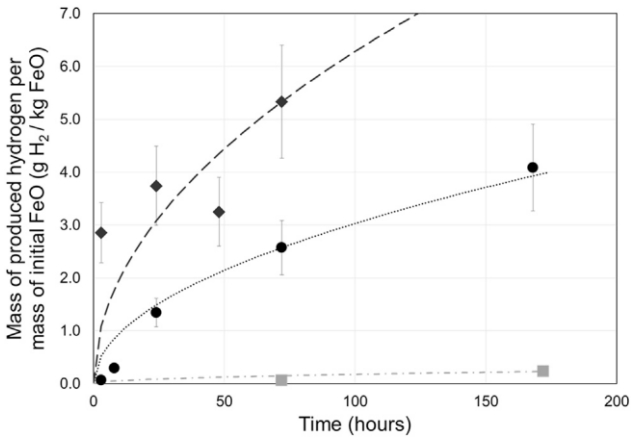

Fig. 4 e Hydrogen production from FeOeH$_2$O in gold capsule system at 373 (square), 423 (circle) and 473 K (diamond) e 30 MPa.

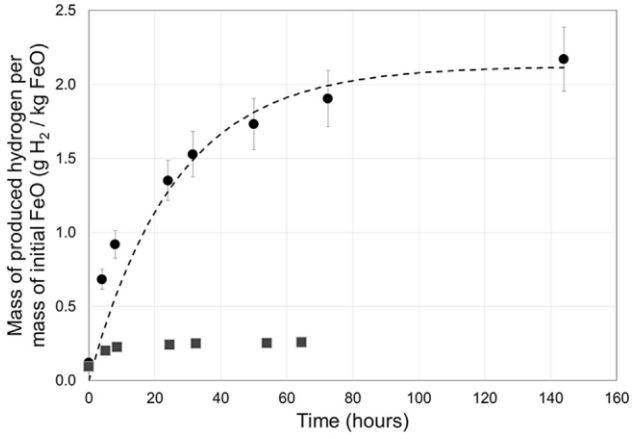

Fig. 5 e Corrected H_2 production kinetics in pure water at 423 K (square) and 573 K (circle); Dashed line corresponds to a pseudo first-order kinetic fit to the 573 K data, log k is estimated to ¡3.26.

can be seen on Fig. 6a that [$Fe^{2þ}$] of 0.02 and 0.01 mol/L are the expected concentrations at FeO and Fe_3O_4 saturation, respectively, in the conditions of the experiment.

Evolution of H_2 production (Fig. 6b) is characterized by a first step of fast production, again within the 10 first hours. About 8.06 g of H_2 were produced per kg of sample during this step, equivalent to a reaction progress of 87%. After this first step, dihydrogen was no longer produced in the gas phase. A small decrease was even observed which is attributed to H_2 removal by gas sampling. Indeed, for each gas sampling, estimated to 27 mL, the total pressure is lowered and part of hydrogen is removed from the experimental system. Hydrogen partial pressure, i.e., its concentration, remains constant even though its molar amount is reduced. H_2 production data presented on Fig. 6b are corrected accordingly.

Characterization of the solid products

XRPD on recovered solid samples indicates, beside wüstite and magnetite, the production of goethite, FeO(OH) and, possibly, lepidocrocite (Table 1). Inspection of the run products with FE-SEM in back-scattered electron mode allowed to distinguish between FeO and magnetite. FeO of higher average atomic number is brighter than magnetite (Fig. 7a). Residual iron metal particles were found to occur as bright spots within FeO grains.

FeO oxidation in acetic acid proceeded from FeO grain rim to core either through progressive replacement of the FeO grains without significant morphological change (Fig. 7a), this process will be called pseudomorphic replacement in the following or by FeO dissolution (Fig. 7b) followed by the precipitation of coronae of magnetite nanoparticles (Fig. 7c and d). Magnetite precipitation was also observed with the formation of nanoparticle aggregates (Fig. 8a). Oxidation through dissolution and precipitation dominates in samples produced in the sampling autoclave. Residual FeO recovered from capsule experiments preferentially shows pseudomorphic replacement pointing therefore towards a possible role of stirring on the oxidation reaction process. In pure water, oxidized products occurred as a multitude of dendrites growing pervasively within the FeO grains (Fig. 7g and h). Comparison at the same magnification between residual FeO grains recovered from both acetic acid and distillated water experiments (APAc-H2-150 and APW-H2-

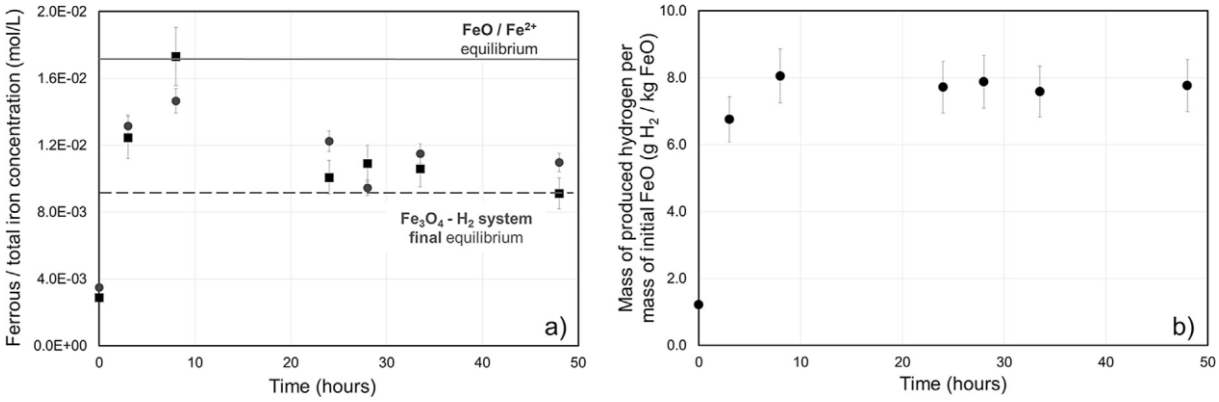

Fig. 6 e Time-resolved monitoring of of aqueous Fe and H_2 of the 423 Ke15 MPa experiment with a 0.05 mol/L acetic acid solution (a) aqueous iron (II þ III) concentration from ICP data (circle) and UV spectrophotometry (square); (b) Corrected H_2 production as measured by GC.

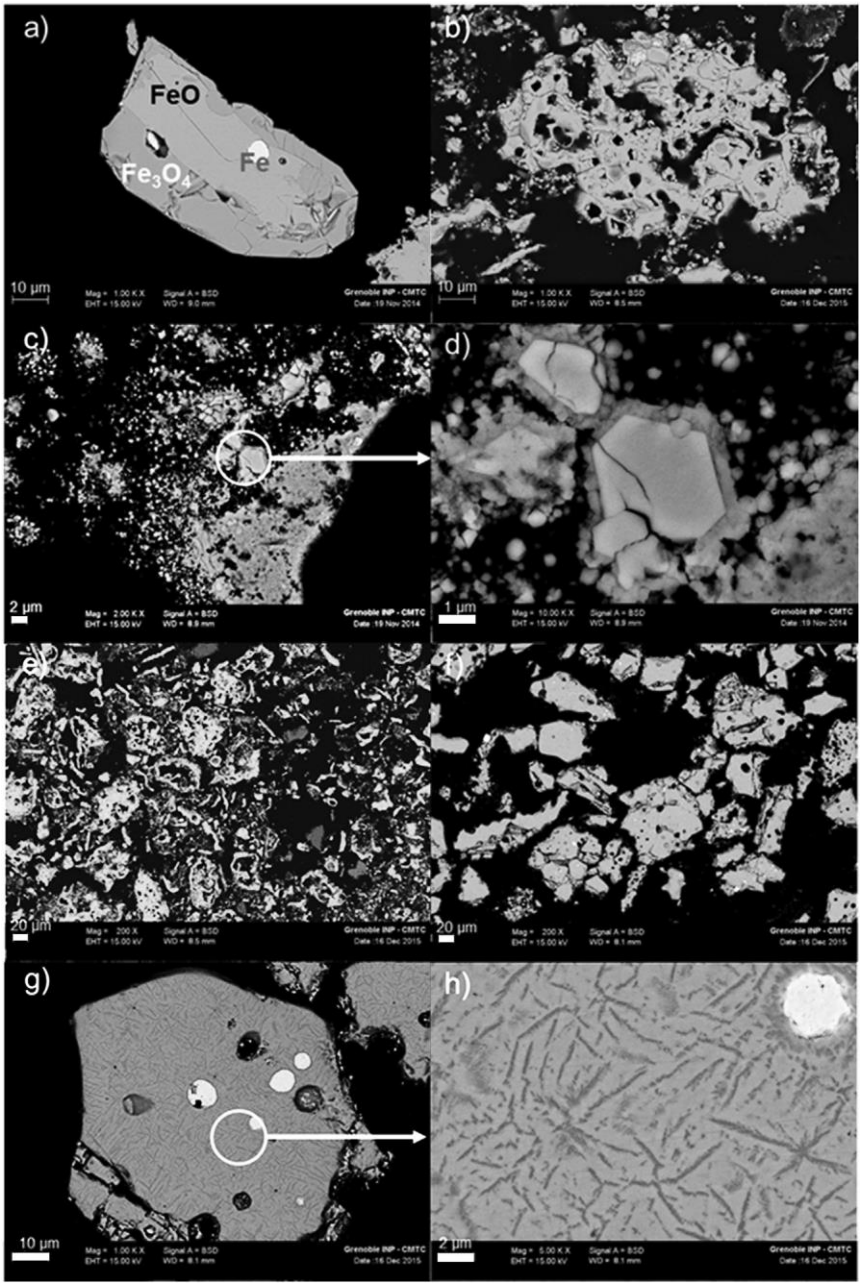

Fig. 7 e FE-SEM back-scattered imaging of the experimental products. a) and b) FeO oxidation features at the grain scale in acetic acid in gold capsule (CAc-H2-2) and sampling autoclave (APAc-H2-150), respectively; c) and d) nanomagnetite covering residual FeO grains (CAc-H2-14); e) and f) FeO oxidation features at the sample scale in acetic acid (APAc-H2-150) and water (APW-H2-300), respectively; g) and h) microtextural details of the FeO (light grey) replacement by Fe_3O_4 (dark grey) in water (APW-H2-300). Experimental conditions for each sample are found in Table 1.

300 respectively, Table 1) are presented on Fig. 7e and f. Particle sizes close to initial (50e100 mm) are still present in both samples, however, whereas particles have nicely kept their shape in water, in acetic acid particles are split up and new reactive surface area has been created.

Goethite, FeO(OH), was detected by XRPD in about half of the experiments performed with acetic acid (Table 1). Goethite grains were easily identified by FE-SEM due to their lower average atomic number and their distinctive morphology (needles or very thin plates, Fig. 9). Goethite was mainly found at the interface between sample and gold-capsule wall. Lepidocrocite was detected using XRPD in samples with comparatively higher hydrogen yield.

In acetic acid experiments, nanoparticles of magnetite were observed included in a carbon matrix (Fig. 8b), suggesting that the carbon-rich compound precipitated during or after FeO oxidation. EDS data and electron diffraction indicated that this solid is composed of amorphous carbon. This lack of crystallinity explains why this solid was not identified by X-ray powder diffraction. To quantify the amount of amorphous

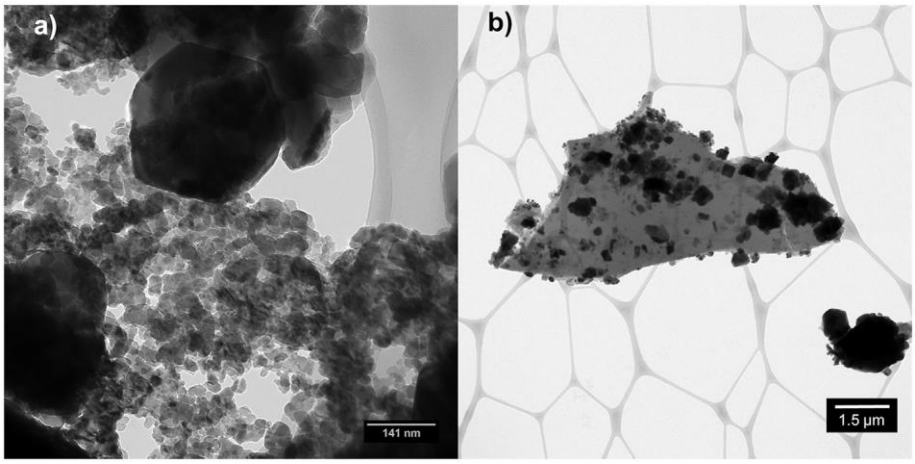

Fig. 8 e TEM images of sample APAc-H2-150. a) Magnetite nanoparticle aggregates; b) inclusions of magnetite nanoparticles in an amorphous carbon phase.

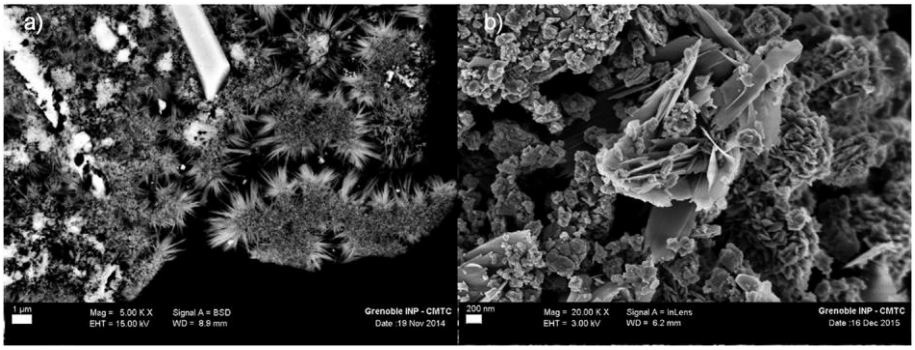

Fig. 9 e FE-SEM images of goethite (a) CAc-H2-14 in back-scattered mode, (b) CAc-H2-12 in secondary electron mode.

carbon, carbon elementary analysis was conducted and returned a carbon mass proportion of 1e1.5%$_w$. Solid carbon has been detected in both capsule and sampling autoclave runs (CAc-H2_03 and APAc-H2-150 samples).

Effect of calcium addition

In order to simulate the oxidation behavior of FeO in steel slags, CaO, which is a major component of steel slag, was added to wüstite. Two mixtures of FeO e $Ca(OH)_2$ (portlandite), and FeO e $CaCO_3$ (calcite), in a mass ratio of 1:1 were run in gold sealed capsules with 0.05 mol/L acetic acid at 423 Ke30 MPa for 3 days. A third capsule containing FeO and pure water was also run in parallel as a reference. Corresponding H_2 yields are presented in Fig. 10. The addition of calcium either as hydroxide or carbonate clearly inhibited FeO oxidation, hydrogen production was very low, i.e., about two orders of magnitude lower than in the Ca-free system under the same conditions (Fig. 10).

Discussion

Effect of acidic conditions and temperature on H_2 yield

At 423 K, H_2 is only produced within the first 10 h to an amount which corresponds to 3% reaction progress. Minor magnetite was identified by XRPD among residual FeO. After this first H_2 production stage and until the end of the run (65 h), no more H_2 is produced. This type of H_2 production behavior is interpreted as either due to (1) the dissolution/ oxidation of small FeO particles with high surface area

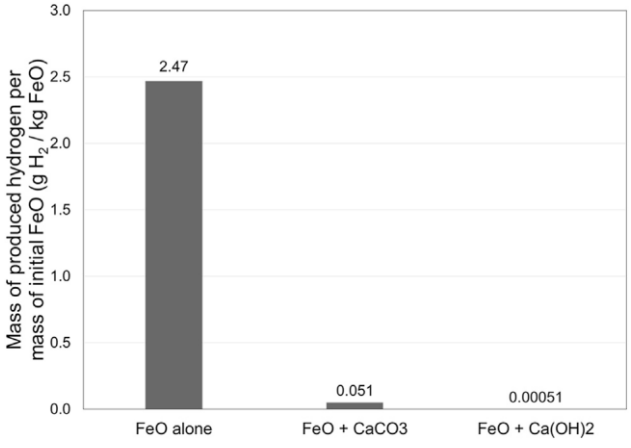

In pure water, hydrogen production through FeO aqueous oxidation has been monitored in a sampling autoclave at two temperatures, 423 and 573 K (Fig. 5), at a pH of ca. 6 (Table 1).

Fig. 10 e Effect of the addition of calcium to FeO as either portlandite or calcite on the H_2 yield in a 0.05 mol/L acetic acid solution at 423 K e 30 MPa for 3 days.

mixed with the 50e100 mm fraction, (2) the reaction of residual grains of Fe metal or (3) the preferential dissolution (and oxidation) of high-energy sites at the surface of FeO grains. Consequently, it will be considered here that FeO grains in the 50e100 mm size range do not react with water to produce H_2 in the presence of pure water at 423 K at the timescale of a day.

At 573 K, within the first 10 h, dihydrogen production kinetics is four times higher than at 423 K. By contrast to the 423 K experiment, H_2 is still produced after 10 h at a rate which decreases progressively with time (Fig. 5). After 144 h, a reaction progress of 23% is attained. At the micro-scale, FeO oxidation into magnetite is mainly localized in channels homogeneously distributed in the bulk of the grain (Fig. 7h). Magnetite seems to nucleate on structural defects or cracks. Magnetite formation might be related to an auto-oxidation process as already emphasized for Fe(II) aqueous oxidation at the surface of hydrous iron oxides [19]. Whatever the exact oxidation process, formation of magnetite in the bulk of the FeO grains suggests that oxidation kinetics will not be directly related to the surface area of the FeO starting material. In other words, the reduction of the FeO grain size by grinding might not significantly enhance the reaction kinetics.

FeO oxidation was found to be strongly enhanced in the presence of acetic acid (Fig. 6b). Whereas we showed that FeO grains in the 50e100 mm size range do not react with pure water at 423 K, the same experience performed with 0.05 mol/L of acetic acid (starting pH of 3) reached completion (or near completion) within 10 h.

For temperatures in the 293e303 K range in acidic solutions, dissolution rates of simple oxide minerals were found to be proportional to $\delta a_{H^+}\Phi^{0.40:7}$ by Casey et al. (1993, [23]) where $\delta a_{H^+}\Phi$ denotes H^+ activity. This means that, at ambient conditions, a pH decrease by 3 units between pure water and acetic acid experiments is expected to result in a higher dissolution rate by 1e2 orders of magnitude. The effect of temperature and pressure on the dependency of FeO dissolution rate with pH is not known but a difference by 1e2 orders of magnitude for a difference of 3 pH units is consistent with what is observed here at 423 Ke15 MPa. Preliminary tests in sealed gold capsules containing the same unsieved FeO powder along with three different acidic solutions, acetic, oxalic and hydrochloric at pH ¼ 3 gave contrasted H_2 yields at 423 K and 30 MPa (Fig. 3). Actually, this result is not inconsistent with a first order pH effect on FeO dissolution (and oxidation). First, aqueous oxalic acid is thermally unstable. A reaction constant of 10^9 is calculated for oxalic acid decomposition into $2CO_{2(aq)}$ and $1H_{2(aq)}$ at 423 K and 20 MPa. Crossey (1991, [24]) showed that at 433 K, pH ¼ 3.6, about half the initial oxalate is decomposed after 45 h. On the contrary, aqueous acetic acid is stable at high temperature with a decomposition reaction constant of 10^{17} ($C_2H_4O_{2(aq)} + 2H_2O_{(l)} \rightarrow 2CO_{2(aq)} + 4H_{2(aq)}$). In the absence of a catalyst, Bell et al. (1994, [25]) showed that at a temperature as high as 608 K, only 1% of the initial acetic acid solution (ca. 1 mol/L) decomposed after 10 days. It can therefore be considered acetic acid decomposition as negligible in our experiment performed at 423 K for 11 days. H_2 production is higher by 1.5 order of magnitude for acetic acid solution (initial pH ¼ 3) than for HCl solution (initial pH ¼ 3). The in-situ pH of these acidic solution at magnetite saturation is calculated, at 423 K and 30 MPa, to be 4.7 and 5.2, respectively. Either this H_2 production difference is due to a proton promoted Fe(II) dissolution in relation to the 0.5 pH unit difference between the two solutions or it is due to a ligand-promoted Fe(II) dissolution by acetic acid. Whereas oxalate-ligand has been showed to enhance the dissolution of Fe(III) compounds [26], acetate has a pronounced affinity for Fe(II) to form a complex such as $FeCH_3COOH^+$ which becomes the dominant Fe(II) aqueous form for pH > 5 (Fig. 11). Dissolution of iron-bearing silicates in acetic acid solutions seems to converge towards a proton-promoted rather than a ligand-promoted dissolution [27,28]. However, due the stability of acetate e iron aqueous complexes at 423 K (Fig. 11) and above, ligand-promoted Fe(II) dissolution in acetic acid solutions at high pressure and temperature cannot be ruled out.

H_2 production and Fe(II) dissolution in acetic acid at 423 K have both been monitored in the sampling autoclave at 150 MPa. Fe(II) concentration reached a maximum after 10 h which corresponds to wüstite saturation. Then, Fe(II) decreased to reach magnetite saturation in a time interval of less than 15 h (Fig. 6a). All the H_2 is produced within these first 10 h (Fig. 6b). XRPD analysis of post-mortem solid indicates full conversion of FeO into Fe_3O_4.

It can be concluded from these results that (1) FeO has fully reacted within the first 10 h of experiments, (2) as long as FeO is present, it controls the aqueous Fe(II) content, (3) most, if not all, of both magnetite and H_2 is produced within the first 10 h. Consequently, FeO dissolution step is faster than Fe(II) oxidation and/or magnetite precipitation step(s) which

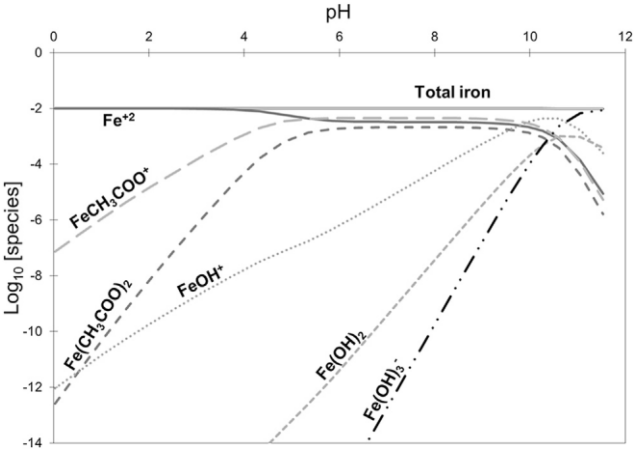

therefore occur to be the rate-limiting step(s). This limitation is confirmed by the formation of magnetite nanoparticles. The quick dissolution step prevents magnetite to grow leading to aqueous iron oversaturation and the forced precipitation of magnetite as nanoparticles (Fig. 8a). However, at the resolu-tion of our sampling frequency, the experimental conditions appear to be close to optimal since all these reaction steps seem to proceed at similar rates since FeO transformation into Fe_3O_4 is achieved when aqueous Fe(II) reaches FeO saturation. If the kinetics of the steps leading to the formation of magnetite would have been lower then H_2 (and magnetite)

Fig. 11 e Speciation of aqueous iron (II) at 423 Ke15 MPa assuming 0.01 mol/L of total Fe (no mineral equilibria) in 0.05 mol/L of acetic acid.

would have still been produced after FeO saturation had been achieved. Experiments performed in gold capsules with acetic acid at 0.005, 0.05 and 0.5 mol/L under identical conditions (423 K, 10 days, 30 MPa) confirmed that near optimal conditions have been reached for a concentration of 0.05 mol/L at 423 K. As a matter of fact, whereas H_2 yield increased by about two orders of magnitude between 0.005 and 0.05 mol/L experiments, H_2 yield between 0.05 and 0.5 mol/L is not significantly different.

Iron dissolution flux has been calculated according to method detailed by Jang et al. (2009, [16]) from iron (II) concentration data (Fig. 6a). The slope, s, has been evaluated from the two first dissolution points, d represents the mass concentration of FeO and A the surface area measured by N_2-BET.

$$F = \frac{s}{dA} \quad (3)$$

A log dissolution flux (mol/m^2/s) of 3.3 has been obtained for our experimental conditions. At ambient conditions, for an equivalent pH of 4.7, a log flux (mol/m^2/s) value of 8.0 is expected. Such a difference may be related to the thermally activated character of the dissolution process. Based on these two dissolution fluxes at two different temperatures, an activation energy of ca. 90 kJ/mol is calculated, which is in good agreement with values obtained for iron (III) oxides dissolution [29]. Moreover, iron solubility is largely increased with the addition of acetic acid at 423 K and 30 MPa from $2.2\ 10^{-6}$ mol/L in water to $9.1\ 10^{-3}$ mol/L in a 0.05 mol/L acetic acid solution.

In parallel to the effect of pH, we confirmed the result of Malvoisin et al. (2013, [7]) obtained on steel slags which is that hydrothermal hydrogen production is a thermally activated process. In water, experiments performed in the sampling autoclave led to a maximum of produced hydrogen 9 times higher at 573 K than at 423 K (Fig. 5). Temperature is expected to play a role on both oxidation and dissolution rates, two thermally activated processes. However, even by applying temperature from 423 to 573 K in water, rate and maximum hydrogen production remains far lower than observed at 423 K in acetic acid (Fig. 6b). In other word, in order to attain significant kinetics improvement, the use of mild acidic solvent is a far better solution than increasing temperature.

H_2 yield difference between capsule and sampling autoclave

H_2 yield differences have been encountered between capsule and sampling autoclave experiments. Under the same conditions of temperature, pressure and acetic acid concentration, total amount of dihydrogen produced after 8 h is 27 times lower for experiments conducted in capsules (Fig. 4) than for experiments in the sampling autoclave (Fig. 6b). The overall shape of the H_2 production curves is also different with a lower production rate at the beginning of the run in the gold capsules. The reaction textures are also different and involve pseudomorphic replacement of starting FeO grains. The differences in H_2 yield between the two experimental methods can be potentially accounted for by (1) a large difference in importantly (3), the lack of stirring. Indeed, stirring enhances iron dissolution, identified as limiting factor to dihydrogen production, through homogenization of the solution. Whatever the nature of the solvent, oxidation features of iron oxide grains recovered from gold capsules also occurred to be different. In particular, oxidation is found to mainly proceed according to a progressive pseudomorphic replacement of the initial FeO grains (Fig. 7a). Stirring has also a mechanical effect which could account for the reaction texture differences observed between stirred and static experiments.

Goethite and solid carbon

Goethite, FeO(OH), was observed by XPRD in some of the samples produced in acetic acid solutions (Fig. 9). As an Fe(III) hydroxide, the precipitation of which, instead of magnetite, can potentially improve the H_2 yield. However, goethite was only detected in experiments run in gold capsules, mainly attached to the capsule walls. Its proportion was not quantified but seemed low compared to those of magnetite and wüstite. At the end of run, gold capsules were dried at 353 K without washing contrarily to the powder samples recovered from the sampling autoclave. As thermodynamics predicts that magnetite should be the only stable iron oxide/hydroxide phase in the investigated hydrothermal conditions, goethite formation is likely to be the result of evaporating Fe-rich acetic acid solution in air.

Nominally, the only source of carbon in our experimental system is acetic acid, through the reaction,

$$CH_3COOH_{(aq)} = 2C_{(s)} + 2H_2O_{(l)}. \quad (4)$$

A possible route for the formation of solid carbon is the thermal decomposition of acetic acid

$$CH_3COOH_{(aq)} = 2CO_{2(g)} + 4H_{2(g)} \quad (5)$$

their respective solid/solution mass ratio (1:200 in sampling autoclave and 1:1 in gold capsules), (2) the likely absence of a gas phase in experiments performed in capsules and, most

followed by the reduction of CO_2 into solid carbon. Magne-tite surface has been shown to catalyze that later step under similar P-T conditions [30]. However, in contrast with the re-sults of Milesi et al. (2015, [30]), carbon has been only observed in magnetite-carbon agglomerates, and no carbon coating on magnetite grains has been observed in the sample. It should be noted that the overall C forming Reaction (4) has no direct impact on the H_2 budget. It can be calculated that $4\%_{mol}$ of acetic acid must have decomposed according to Reaction (4) in order to account for the 1e2 weight percent of carbon analyzed in sample (APAc-H2-150). This estimate is signifi-cantly higher than the results by Bell et al. (1994, [25]), already mentioned, on the kinetics of acetic acid decomposition without catalyst. A possible catalytic effect of magnetite nanoparticles may be put forward in our experiments.

From FeO to steel slag

Steel slags contain in average $46\%_w$ of CaO [31]. Initially pre-sent in the form of lime, CaO, in freshly produced slags, aging of the slag in air leads to the formation of portlandite, $Ca(OH)_2$
and calcium carbonate, $CaCO_3$.

Three experiments performed at 423 K and 30 MPa for 3 days in gold capsules with pure FeO, FeO þ $CaCO_3$ and FeO þ $Ca(OH)_2$ in a 0.05 mol/L acetic acid solution yielded contrasted H_2 production of 1.234, 0.025 and 0.0005 g H_2/FeO kg, respectively (Fig. 10). The addition of a Ca-phase such as $Ca(OH)_2$ or $CaCO_3$, in the presence of acetic acid strongly modifies the speciation and pH of the aqueous solution. In particular, when portlandite is present, along with Fe_3O_4, the pH of the solution is high (pH ¼ 9.1) due to the relatively high solubility of $Ca(OH)_2$. In the case where calcite is the only Ca-bearing solid, pH is buffered to a value of 5.8, i.e., slightly above the measured final pH in the Ca-free Fe_3O_4 e acetic acid system (pH ¼ 4.7). In addition to the increase of pH which will tend to slow down the FeO dissolution (see discussion above), the total amount of aqueous Fe(II) in equilibrium with Fe_3O_4 is drastically lowered, from ca 10^2 mol/L to 10^6 mol/L in the presence of $CaCO_3$ and down to 10^{11} mol/ L when $Ca(OH)_2$ is present.

Conclusion

For the sake of testing factors that could increase the kinetics of H_2 production by hydrothermal treatment of steel slags according to the $3\,FeO_{(s)} + H_2O_{(l)} = Fe_3O_{4(s)} + H_{2(aq)}$ reaction [7], pure FeO was used as model compound and tested in the 373e573 K range in the presence of mild acidic solutions.

The effect on the kinetics of H_2 production from FeO of acetic acid at concentrations far below that of vinegar is remarkably strong. In 0.05 mol/L acetic acid at 423 K, FeO oxidation reaches near completion within 10 h whereas, in pure water, H_2 yield is negligible, even after 65 h. We identified FeO dissolution as the rate-limiting step; therefore, the kinetics effect of acetic acid is primarily interpreted as related to the dependency of FeO dissolution rate with pH. A log dissolution flux (mol/m^2/s) as high as 3.3 has been obtained at 423 K with an acetic acid concentration of 0.05 mol/L. At the microscale, fast reaction kinetics is associated with a dissolution/precipitation process which gives rise to a multitude of small magnetite particles covering the fast dissolving FeO grains. Hydrothermal H_2 production from FeO oxidation is thermally activated; however, the kinetics enhancement associated with the use of mild acidic solutions is found to be enormous in comparison to that of temperature. Acetic acid being thermally stable, it allows the combination of acidic conditions at high temperature. In order to take advantage of the positive effect of acetic acid on H_2 yield, solutions are being explored to maintain acidic conditions in the presence of Ca-bearing phases which are ubiquitous in steel slags. In particular the presence $Ca(OH)_2$ should be avoided since it tends to neutralize acetic acid and impose basic conditions which have a dramatic effect on H_2 production.

Acknowledgements

This work is supported by CNRS through the "Mission Interdisciplinaire: Defi Transition Energetique: Ressources, Societe, Environnement e ENRS" program. This work is part of the HyMag'In project funded by the SATT Linksium (Grenoble). Labex OSUG@2020 is also thanked for financial support. The authors would like to thank Moulay-Tahar Sougrati for Mössbauer spectroscopy. Valerie Magnin is thanked for the BET measurement at ISTerre.

references

[1] Ni M, Leung DY, Leung MK, Sumathy K. An overview of hydrogen production from biomass. Fuel Process Technol 2006;87(5):461e72.
[2] Kodama T, Gokon N. Thermochemical cycles for high-temperature solar hydrogen production. Chem Rev 2007;107(10):4048e77.
[3] Turner J, Sverdrup G, Mann MK, Maness P-C, Kroposki B, Ghirardi M, et al. Renewable hydrogen production. Int J Energy Res 2008;32(5):379e407.
[4] Klein F, Bach W, McCollom TM. Compositional controls on hydrogen generation during serpentinization of ultramafic rocks. Lithos 2013;178:55e69.
[5] Charlou J, Donval J, Fouquet Y, Jean-Baptiste P, Holm N. Geochemistry of high H_2 and CH_4 vent fluids issuing from ultramafic rocks at the Rainbow hydrothermal field (3614ºN, MAR). Chem Geol 2002;191(4):345e59.
[6] Marcaillou C, Munoz M, Vidal O, Parra T, Harfouche M. Mineralogical evidence for H_2 degassing during serpentinization at 300C/300 bar. Earth Planet Sci Lett 2011;303(3e4):281e90.
[7] Malvoisin B, Brunet F, Carlut J, Montes-Hernandez G, Findling N, Lanson M, et al. High-purity hydrogen gas from the reaction between BOF steel slag and water in the 473e673 K range. Int J Hydrogen Energy 2013;38(18):7382e93.
[8] Hacker V, Fankhauser R, Faleschini G, Fuchs H, Friedrich K, Muhr M, et al. Hydrogen production by steam e iron process. J Power Sources 2000;86(1e2):531e5.
[9] Lorente E, Pena JA, Herguido J. Cycle behaviour of iron ores in the steam-iron process. Int J Hydrogen Energy 2011;36(12):7043e50.
[10] Lorente E, Herguido J, Pena JA. Steam-iron process: influence of steam on the kinetics of iron oxide reduction. Int J Hydrogen Energy 2011;36(21):13425e34.
[11] Stehle RC, Bobek MM, Hooper R, Hahn DW. Oxidation reaction kinetics for the steam-iron process in support of hydrogen production. Int J Hydrogen Energy 2011;36(23):15125e35.
[12] Chiesa P, Lozza G, Malandrino A, Romano M, Piccolo V. Three-reactors chemical looping process for hydrogen production. Int J Hydrogen Energy 2008;33(9):2233e45.
[13] Chen S, Shi Q, Xue Z, Sun X, Xiang W. Experimental investigation of chemical-looping hydrogen generation using Al_2O_3 or TiO_2-supported iron oxides in a batch fluidized bed. Int J Hydrogen Energy 2011;36(15):8915e26.
[14] Kang K-S, Kim C-H, Bae K-K, Cho W-C, Kim S-H, Park C-S. Oxygen-carrier selection and thermal analysis of the chemical-looping process for hydrogen production. Int J Hydrogen Energy 2010;35(22):12246e54.
[15] Ryden M, Arjmand M. Continuous hydrogen production via the steam e iron reaction by chemical looping in a circulating fluidized-bed reactor. Int J Hydrogen Energy 2012;37(6):4843e54.
[16] Jang J-H, Brantley SL. Investigation of wüstite (FeO) dissolution: implications for reductive dissolution of ferric oxides. Environ Sci Technol 2009;43(4):1086e90.
[17] Blesa MA, Matijevic E. Phase transformations of iron oxides, oxohydroxides, and hydrous oxides in aqueous media. Adv Colloid Interface Sci 1989;29(3e4):173e221.
[18] Morgan B, Lahav O. The effect of pH on the kinetics of spontaneous Fe(II) oxidation by O2 in aqueous

solutione basic principles and a simple heuristic description. Chemosphere 2007;68(11):2080e4.
[19] Wehrli B, Sulzberger B, Stumm W. Redox processes catalyzed by hydrous oxide surfaces. Chem Geol 1989;78(3e4):167e79.
[20] Domingo C, Rodriguez-Clemente R, Blesa M. Nature and reactivity of intermediates in the auto-oxidation of iron (II) in aqueous acid media. Solid State Ionics 1993;59(3e4):187e95.
[21] Brunet F, Chopin C. Bearthite, $Ca_2Al(PO_4)_2OH$: stability, thermodynamic properties and phase relations. Contrib Mineral Petrol 1995;121(3):258e66.
[22] Johnson JW, Oelkers EH, Helgeson HC. SUPCRT92: a software package for calculating the standard molal thermodynamic properties of minerals, gases, aqueous species, and reactions from 1 to 5000 bar and 0 to 1000C. Comput Geosci 1992;18(7):899e 947.
[23] Casey WH, Banfield JF, Westrich HR, McLaughlin L. What do dissolution experiments tell us about natural weathering? Chem Geol 1993;105(1e3):1e15.
[24] Crossey LJ. Thermal degradation of aqueous oxalate species. Geochim Cosmochim Acta 1991;55(6):1515e27.
[25] Bell JL, Palmer DA, Barnes HL, Drummond SE. Thermal decomposition of acetate: III. Catalysis by mineral surfaces. Geochim Cosmochim Acta 1994;58(19):4155e77.
[26] Chen H, Grassian VH. Iron dissolution of dust source materials during simulated acidic processing: the effect of sulfuric, acetic, and oxalic acids. Environ Sci Technol 2013;47(18):10312e21.
[27] Hamer M, Graham RC, Amrhein C, Bozhilov KN. Dissolution of ripidolite (Mg, Fe-Chlorite) in organic and inorganic acid solutions. Soil Sci Soc Am J 2003;67(2):654.
[28] Stumm W. Reactivity at the mineral-water interface: dissolution and inhibition. Colloids Surf A Physicochem Eng Asp 1997;120(1e3):143e66.
[29] Schwertmann U. Solubility and dissolution of iron oxides. Plant Soil 1991;130(1e2):1e25.
[30] Milesi V, Guyot F, Brunet F, Richard L, Recham N, Benedetti M, et al. Formation of CO_2, H_2 and condensed carbon from siderite dissolution in the 200e300C range and at 50 MPa. Geochim Cosmochim Acta 2015;154:201e11.
[31] Yildirim IZ, Prezzi M. Chemical, mineralogical, and morphological properties of steel slag. Adv Civil Eng 2011;2011(2):1e13.
[32] Parkhurst DL, Appelo CAJ. User's Guide to PhreeqC (Version 2)d A computer program for speciation, batch-reaction, one-dimensional transport, and inverse geochemical calculations. 1999. U.S. Geological Survey, Water-Resources Investigations Report 99-4259, Denver, CO.